# Prediction of Shear Strength of UHPC Beam with Small Shear Span to Depth Ratios Based on Modified MCFT

**Linyun Zhou** ( 101300072@seu.edu.cn )
Southeast University
**Shui Wan**
Southeast University

**Research Article**

**Keywords:** UHPC, Shear capacity, MCFT, crack angle, shear span to depth ratios

**Posted Date:** January 6th, 2022

**DOI:** https://doi.org/10.21203/rs.3.rs-1216609/v1

# Prediction of shear strength of UHPC beam with small shear span to depth ratios based on modified MCFT

Linyun Zhou* Shui Wan

* Linyun Zhou：Post-Doc, School of Transportation, Southeast University, 2 Sipailou, Nanjing, China, 210096, 101300072@seu.edu.cn.

## Abstract

Ultra-high performance concrete (UHPC) has been gradually used in structure engineering due to its excellent mechanical performance, however, predicting the shear capacity of the UHPC beams is still a challenge, especially for the beams with small shear span to depth ratios. To address this issue, this paper devotes to developing a rational model to predict the shear capacity of the UHPC beams with stirrups based on the modified compression field theory (MCFT) and plastic theory. The shear force will be balanced by the stirrups, matrix, fibers and shear compression zone. The contribution of stirrups, matrix and fibers on shear capacity can be predicted by MCFT, and the contribution of compression zone is determined based on plastic theory. 12 UHPC beams was designed and tested to validate the proposed model. It can be found that the predictions agree well with test results, while the current design codes, including SETRA-AFGC and SIA, give overly conservative values for UHPC beams when the shear to span is less than 2.5.

**Keywords:** UHPC, Shear capacity, MCFT, crack angle, shear span to depth ratios

# Introduction

Ultra-high performance concrete (UHPC) has been gradually used in bridge engineering due to its higher compression strength and better crack resistance [1]. Over the past two decades, many efforts had been done on the composition [2], mechanical properties [3], and structural behavior of UHPC members [4]. To date, effective methods for predicting the bending behavior of UHPC beams had been developed based on the plane section assumption, and validated by various test results [5], which had been included in the current design codes [6-8]. While, as for the shear behavior of the UHPC beams, it seems that the estimation calculated based on the design codes had a great discrepancy with the experimental results [9-11], especially for the UHPC beams with small shear span to depth ratios.

Actually, the shear behavior of UHPC beams was effected by many factors, such as details of reinforcement bars and stirrups, shear span to depth ratios. Nowadays, five main methods were developed to predict the shear strength of the UHPC beams, that is, empirical method, truss model, limit equilibrium theory, plastic theory and modified compression field theory (MCFT). Empirical equations were proposed to predict the shear strength of the UHPC beams based on the test results [12], however, the coefficients in the equations lacked physical meaning and were hard to define, which lead a very limited application. The truss model was widely accepted to estimate the shear capacity of the beams. Based on the rotating-angle softened truss model, the contribution of the matrix, stirrups and steel fibers to the shear strength can be determined respectively, and then the shear strength of UHPC beams can be

estimated. This method was included in the design codes of JSCE [6], AFGC [7] and SIA [8]. In 2017, Ma et al. [13] collected the tested shear capacity of 51 UHPC beams, and they stated that the truss model cannot predict the shear capacity of UHPC beams with satisfactory accuracy, especially for the UHPC beams with small shear span to depth ratios ($1<\lambda<2$), the maximum relative error was up to 28%.

As for the limit equilibrium theory, the shear force was assumed to be balanced by the stirrups, matrix, steel fibers, aggregate interlock forces and friction forces at crack interface, thus the limit equilibrium equations of the two parts divided by the main diagonal crack can be determined following the failure criterion of the UHPC. The shear strength can be obtained by introducing the deformation equations. However, the stress distribution in the shear compression zone and the horizontal projected length of the diagonal crack were hard to determine. In 2014, Xu and Deng. [14] tested a series of UHPC beams with different shear span to depth ratios, and the test results show that the maximum relative errors between the predictions of limit equilibrium theory and test results reached 34% for the UHPC beams with small shear span to depth ratios. As for the method based on the plastic theory, the reinforcement bars and concrete were assumed to the perfect elasto-plastic materials, and then the upper-bound solution obtained by the given yield criterion can be regarded as the shear capacity of UHPC beams. However, the plasticity coefficient was hard to quantify. In 2010, following the plastic theory, Voo et al. [15] proposed equations to estimate the shear capacity of UHPC beam without stirrups. The maximum relative errors of the predictions and test result was up to 25%, because the critical diagonal

65 crack was assumed to approach the top of the beam, and the contribution of the shear
66 compression zone was omitted.

67 The MCFT, proposed by Collins et al. [16], had been widely used as an effective
68 tool to calculate the shear strength of concrete beams, and included in current design
69 codes. In 2010, Charles et al. [17] designed and tested 6 UHPC beams, the study showed
70 that the calculations of MCFT were conservative compared with the test results, the
71 relative error was varied from 19% to 59%. Same conclusions can be found in other
72 related research works [10,11]. The predictions were less than the test results because the
73 contribution of the shear compression zone on shear strength was neglected in MCFT.

74 As can be seen, although there are various of methods to calculate the shear
75 capacity of UHPC beams, the predictions are found to be conservative, especially for
76 UHPC beams with small shear span to depth ratios ($1<\lambda<2$). To this end, this paper
77 devotes to develop a rational model to predict the shear capacity of the UHPC beams
78 with stirrups based on MCFT and plastic theory. The contribution of stirrups, matrix
79 and fibers on shear capacity can be determined by MCFT, and the contribution of
80 compression zone will be determined based on plastic theory.

## 81 Shear strength of UHPC beams

82 As for the UHPC beams at the ultimate limit state, the shear force will be
83 balanced by the stirrups, matrix, fibers and shear compression zone, as shown in Fig.
84 1. Thus the shear strength of UHPC beams can be given by

85 $$V = V_c + V_{sf} + V_{sv} \tag{1}$$

Contribution of the stirrups $V_{sv}$, matrix and fibers $V_{sf}$ can be determined by MCFT, and the contribution of the shear compression zone, $V_c$, will be predicted by the plastic theory.

## Contribution of stirrups and materials based on MCFT

### equilibrium conditions

Fig. 2 shows the stresses station of the UHPC elements under pure shear, where $\nu$ is the shear stress; $f_1$ and $f_2$ are the principal tensile stress and compressive stress of the UHPC elements, respectively; $\theta$ is the crack angle. Based on the assumption that the shear stress, $\nu$, on flat section is uniformly distributed, it can be obtained

$$\nu=\frac{V}{bd_v} \tag{2}$$

in which, $V$ is the shear force, $b$ and $d_v$ are the thickness and internal lever arm of the UHPC beam, respectively.

According to Mohr circle, we have

$$f_1+f_2=\nu(\tan\theta+\cot\theta)=\frac{V}{bd_v}(\tan\theta+\cot\theta) \tag{3}$$

According to the equilibrium condition in the vertical direction, we have

$$A_v f_v=(f_2\sin^2\theta-f_1\cos^2\theta)bs \tag{4}$$

where, $A_v$, $f_v$ and $s$ are the area, stress and spacing of the stirrups, respectively.

Substituting Eq. (3) into Eq. (4), the shear force can be derived by

$$V=\frac{A_v f_v}{s} d_v \cot\theta + f_1 d_v t \cot\theta \tag{5}$$

The first item in the formula can be regarded as the contribution of stirrups ($V_{sv}$) and the second item can be regarded as the contribution of UHPC matrix and fibers ($V_{sf}$).

**compatibility conditions**

Assuming that the principal stress direction is consistent with the strain direction, thus, the average strain of UHPC can be obtained based on the Mohr circle

$$\tan^2\theta=\frac{\varepsilon_x-\varepsilon_2}{\varepsilon_y-\varepsilon_2} \tag{6a}$$

$$\varepsilon_1=\varepsilon_x+\varepsilon_y-\varepsilon_2 \tag{6b}$$

$$\gamma_{xy}=2(\varepsilon_x-\varepsilon_2)\cot\theta \tag{6c}$$

in which, $\varepsilon_1$ and $\varepsilon_2$ are the principal strain of UHPC members parallel to and perpendicular to the crack; $\varepsilon_x$ and $\varepsilon_y$ are the strain in UHPC in longitudinal and transverse direction, respectively; $\gamma_{xy}$ is the shear strain.

**Transmitting forces across cracks**

As for the normal concrete structure, the shear force was balanced by the stirrups and aggregate interlock with cracks, while as for the UHPC, the contribution of fiber shall be taken into account as shown in Fig. 3. According to Stroeven [18], the stress at cracks can be given by

$$\sigma_\theta = \frac{d_f}{3l_f} v_f \tau_f (1+\frac{1}{2}K)(1-\frac{8w}{l_f}) \quad (7)$$

in which, $d_f$ and $l_f$ are the fiber diameter and length, respectively. $v_f$ is the fiber volume fraction, $\tau_f = 1.11(f_{ct})^{1.354}$ is the friction resistance in pullout between fiber and concrete [19]; $K$ defines the degree of planar orientation, which is primarily due to reorientation of fibers caused by filling the mold and by compaction, and can be determined by the SETRA-AFGC [7]. $w = \varepsilon_1 s_\theta$ is the average cracking width, $s_\theta$ is the average crack space and can be obtained by [20]

$$s_\theta = \frac{d_f f_{ct}}{4K v_f \tau_f} \quad (8)$$

According to the equilibrium condition of the cracks

$$\rho_v f_v \cos\theta + f_1 \cos\theta = \rho_v f_{vcr} \cos\theta - f_{ci} \cos\theta + v_{ci} \sin\theta + n_A \sigma_\theta (1+\frac{1}{\tan\theta}) \quad (9)$$

where, $\theta$ is the inclined crack angle; $A_v$ and $f_v$ are the area and average stress of the stirrups; $f_{vcr}$ is the stress of the stirrups at cracks; $f_{ci}$ is the compressive stress at the crack; $n_A$ is the number of fibers in unit area; $v_{ci}$ is the shear stress across the crack.

Moreover, the stress in the reinforcement at a crack cannot exceed the yield strength, that is, the maximum principal tensile stress can be obtained by

$$f_{1\max} = \frac{A_v (f_{vy} - f_v)}{bs} + n_A \sigma_\theta (1+\tan\theta) \quad (10)$$

in which, $f_{vy}$ is the yield strength of the stirrups.

**Constitutive laws for UHPC**

The behavior of the reinforcement bars is assumed to be perfect elasto-plastic, that is, the stress-strain relationships can be given by

$$\sigma_s = E_s \varepsilon_{sx} \le f_{sy} \tag{11}$$

In which， $E_s$ and $f_{sy}$ are the modulus and yield stress of the bars.

According to the research of Yuan [21], the tensile stress-strain relationships for UHPC can be obtained by

$$\sigma_t = \begin{cases} E_c \varepsilon, & \varepsilon \le \varepsilon_{cr} \\ \dfrac{1+0.75\beta}{1+\beta} E_c \varepsilon_{cr}, & \varepsilon > \varepsilon_{cr} \end{cases} \tag{12}$$

in which， $\beta = \sqrt{\dfrac{\varepsilon_1 - \varepsilon_{cr}}{0.005}}$

As for the compression behavior of UHPC, the stress-strain relationships can be given by [22]

$$\sigma_c = f_{2\max} \frac{n\xi - \xi^2}{1+(n\text{-}2)\xi} \tag{13a}$$

$$f_{2\max} = \frac{f_c'}{0.8+113\varepsilon_1} \tag{13b}$$

where， $\xi = \varepsilon / \varepsilon_0$； $\varepsilon_0 = -0.0035$ is the strain of UHPC corresponding to the peak stress; $f_c'$ is the compressive strength of UHPC; $n = E_s / E_c$， $E_c$ and $E_s$ are the Young's modulus and secant modulus at peak, respectively.

## Contribution of compression zone

### UHPC beams with shear and moment

Assuming that the UHPC beams with shear and moments conforms to the plane section assumption as shown in Fig. 4. The tensile stress at the bottom of the UHPC beam caused by the moment will reduce the strain induced by shear force. According to the layer model in MCFT [23], it can be assumed that the longitudinal cross section strain of the beam at the height of $h/3$ is equal to the strain calculated by Eq. (6). Thus, the strain at the cross section can be expressed as follows

$$\frac{\varepsilon_c}{c}=\frac{\varepsilon_x}{2h/3-c}=\frac{\varepsilon_{sx}}{h_0-c}=\frac{\varepsilon_s'}{c-a_s'} \tag{14}$$

in which, $c$ is the height of the compression zone; $\varepsilon_c$ is the compressive strain at the top cross section; $\varepsilon_{sx}$ is the longitudinal strain of the reinforcement bars.

Therefore, $c$ can be derived by

$$c=\frac{2h\varepsilon_c}{3(\varepsilon_x+\varepsilon_c)} \tag{15}$$

According to the stress strain relationships of UHPC, the resultant compressive force can be obtained by

$$F_c=\int_0^c \sigma_c(\varepsilon)bdy=\beta_1 f_c'bc \tag{16}$$

in which, $\beta_1=\frac{\varepsilon_c}{\varepsilon_0}-\frac{1}{3}(\frac{\varepsilon_c}{\varepsilon_0})^2$.

Then, the distance between the compressive force and longitudinal steel can be given by

$$d = h_0 - c + \frac{\int_0^c \sigma b y dy}{2F_c} = h_0 - \frac{(4-\varepsilon_c/\varepsilon_0)c}{(6-2\varepsilon_c/\varepsilon_0)} \tag{17}$$

The moment and axial force at the cross section can be expressed by

$$M_P = F_c d + E_s' A_s' \varepsilon_s' + n_A \sigma_\theta b (h_0 - c)^2 / 2 \tag{18}$$

$$F_P = E_s A_s \varepsilon_{sx} - E_s' A_s' \varepsilon_s' - F_c \tag{19}$$

**Shear force balanced by compression zone**

Compressive stress and shear stress acted on the compressive zone, and the criterion of Mohr-Coulomb with tension cutoff is adopted to characterize the stress state at the ultimate limit state as shown in Fig. 5. The stress in the Mohr circle can be expressed by

$$\sigma = -\sqrt{\tau_{xy}^2 + (\frac{\sigma_y}{2})^2} \sin\phi + \frac{\sigma_y}{2} \tag{20a}$$

$$\tau = \sqrt{\tau_{xy}^2 + (\frac{\sigma_y}{2})^2} \cos\phi \tag{20b}$$

According to the criterion of Mohr-Coulomb

$$\tau = \tau_0 + \sigma \tan\phi \tag{21}$$

Substituting Eq. (20) into Eq. (21), it yields

$$\tau_{xy} = \sqrt{\tau_0^2 \cos^2\phi - \tau_0 \sigma_y \sin\phi \cos\phi - \frac{\cos^2\phi}{4}\sigma_y^2} \tag{22}$$

According to the test results of the UHPC under uniaxial compression, the compressive strength can be expressed by

$$f_c'=2\tau_0(\tan\phi+\sec\phi) \tag{23}$$

in which

$$\sin\phi=\frac{(\frac{0.5f_c'}{\tau_0})^2-1}{(\frac{0.5f_c'}{\tau_0})^2+1} \tag{24}$$

The above equations are available to get

$$\frac{\tau_{xy}}{f_c'}=\sqrt{1+(m-1)\frac{\sigma_y}{f_c'}-m(\frac{\sigma_y}{f_c'})^2} \tag{25}$$

where，the parameters $\tau_0=\sqrt{f_t f_c'/2}$ and $m=f_c'/2f_t$.

According to the experimental research conducted by Xu and Deng [14]，the relationship between tensile strength and compressive strength of UHPC can be expressed by $f_t=0.0353f_c'$. Then the criterion of the UHPC under combined compression and shear can be illustrated as shown in Fig. 6. It can be seen that the criterion for the compression zone can be approximated by

$$\begin{cases}\tau_1=0.07f_c'+0.2\sigma_c & \sigma_c/f_c'\le 0.5\\ \tau_2=0.26f_c'-0.18\sigma_c & 0.5<\sigma_c/f_c'\le 1\end{cases} \tag{26}$$

Then the shear forces balanced by the compression zone can be derived by

$$V_c=\int_0^c \tau b dy=\int_0^{c_1}\tau_1 b dy+\int_{c_1}^{c}\tau_2 b dy \tag{27}$$

in which, $c_1=cf_c'/2E_c\varepsilon_c$.

Then the axial force induced by the shear can be given by

$$F_V=V\cot\theta-f_1 b d_v \tag{28}$$

## Shear strength of UHPC beam based on MCFT

Following the theory of MCFT, and taking into account the contribution of the compression zone, the shear strength of the UHPC beams with shear and moment can be predicted as shown in Fig. 7. The main steps for shear strength prediction of UHPC beams are as follows:

1. Choose a value of $\varepsilon_1$ at which to perform the calculation.

2. The inclination of principal strain is assumed to be $\theta$.

3. The stress of the stirrups is assumed to be $f_v$.

4. Calculate the principal tensile stress of the UHPC elements, $f_1$, based on the constitutive laws for UHPC and estimation the maximum principal tensile stress, $f_{1\max}$, following Eq. (10).

5. Determine the shear contribution of stirrups and UHPC matrix and fibers based on Eq. (5).

6. Estimate the principal compressive stress, $f_2$, via equilibrium conditions, and the maximum stress of the UHPC, $f_{2\max}$, following the constitutive laws. If $f_2 < f_{2\max}$, go to step 7; if not, the UHPC struts crushed, the computation finished.

7. Determine the principal compressive strain, $\varepsilon_2$, according to the constitutive laws, and compute the longitudinal strain, $\varepsilon_x$, and vertical strain, $\varepsilon_y$, of UHPC based on the compatibility equations Eq. (6).

8. Calculate the average stress of stirrup $f_v = E_s\varepsilon_y \le f_{vy}$. If $f_v$ is equal to the assumed value in step 3, go to the next step; if not, go to step 3 and reassumed the stirrup stress.

9. Assume that the longitudinal strain of the UHPC cross section at h/3 is equal to $\varepsilon_x$ calculated in step 7, and the strain of at the top of beam is assumed to be $\varepsilon_c$. Estimate the strain distribution of UHPC cross section based on the plane section assumption.

10. Calculate the moment, $M_P$ and the axial force, $F_P$, at the UHPC cross section induced by the moment based on Eq. (18) and Eq. (19).

11. Determine the shear strength, $V_c$, contributed to the compression zone according to Eq. (16), then the shear strength, $V$, of UHPC beams with shear and moment can be obtained following Eq. (1). If $M_P=Va$, go to step 12; if not, go to step 9 and adjust the value of $\varepsilon_c$.

12. Estimate the axial force induced by the shear according to Eq. (28). If $F_P - F_V=0$, go to next step; if not, go to step 2, and adjust the value of $\theta$.

13. Repeat step 1 to 12 for the next $\varepsilon_1$, the iterative process terminates when the compressive stress of UHPC reaches the value of $f_{2\max}$, or the strain of reinforcement bars reaches the yield stain; the corresponding shear force, $V$, is the shear strength of the UHPC beams.

# Experimental validation

## Test specimens

According to SETRA-AFGC, 12 UHPC beams with different shear span to depth ratios and various shear stirrups were designed to investigate the shear behavior of UHPC beams with small shear span to depth ratios as shown in Fig. 8. The width and

253 height of the specimens were 0.2m and 0.8m, respectively. The longitudinal
254 reinforcement ratio of the specimens was designed to be $\rho$=1.00% to avoid bending
255 failure. Concrete cover and spacing between reinforcement bars were chosen
256 according to the code provisions. The clear spans of the specimens were varied from
257 1.84 m to 2.94 m, and the corresponding shear span to depth ratios were varied from
258 1.17 to 1.96 as listed in Table 2. The volume fraction of steel fibers was designed to
259 be 2% for all specimens, the length and diameter of the steel fibers were 13mm and
260 2mm, respectively.

261 Gravel with a maximum aggregate size of 10 mm was used, and the mix (list in
262 Table 1) was designed to obtain a compressive strength of 120 MPa at 28 days.
263 Aggregates, cement, and water were batched by weight and mixed in a drum mixer.
264 The fibers were introduced last and dispersed uniformly. The $100\times200$ mm concrete
265 cylinder specimens for compressive tests were also cast from the same mixes to
266 determine the compressive strength. Based on the material tests, the modulus of
267 elasticity and compressive strength of UHPC were tested to be $E_c$=42.6GPa and
268 $f_c$=120Mpa, respectively. The diameter of the longitudinal bars and stirrups with
269 yield stress of 400Mpa were set to be 28mm and 8mm.

270 The beams were tested under three-point loading condition as shown in Fig. 9.
271 All of the test specimens were monotonically loaded over the full thickness so that the
272 specimens would behave in two dimensions. Surface cracks were located by visual
273 observation, and the monitoring of strain gauge data was placed on the key
274 reinforcement as shown in Fig. 8. Dial gauges of 0.01 mm accuracy were placed on

the key locations to measure the deformation, average compressive strain and tensile strain of reinforced UHPC beams throughout the loading process.

**Behavior of UHPC beams under shear force**

For all specimens, test events progressed very similarly as indicated in Fig. 10. As for the specimen of B9 with the shear span ratio $\lambda$=1.74, the load-deformation relationships obtained from dial gauges indicated that the beam exhibited similar linear behavior from initial loading to the occurrence of the first cracking as shown in Fig. 11, with the increment of shear force, a large number of bending cracks occurred at bottom of the beam, and propagated slowly towards the top of the beam, as a result, the stiffness of the beam gradually decreased. It also should be noted that the value of dial gauge placed on the web at the mid shear span to monitor the vertical strain of the UHPC beams, was unchanged until the occurrence of the first cracking as shown in Fig.12, which means that the shear force transferred from the loading point to the supports mainly through the arch action prior to cracking, moreover, the tensile tie of the truss action will move towards to the supports after cracking. When the load is $P$=822kN, a diagonal crack occurred and progressed along the compressive stress trajectories in the shear span. Thereafter, numerous of parallel diagonal cracks occurred in the web, and the crack spacing and crack width were small due to the existence of the steel fiber. Approaching the load of $P$=3443kN, the vertical strain measured by the dial gauges indicated that the stirrups reached the yield strain as shown in Fig. 12, that is, the shear compression failure happened and the

296 corresponding external force was the shear strength of the UHPC beams. With the
297 load increasing, the main crack propagated quickly towards the loading point, and the
298 reinforcement bars appeared rupture and the steel finer pulled out finally.

299 **Shear strength**

300 As stated before, when the stress of the UHPC reached the compressive strength
301 or the strain of the reinforcement bars arrived at the yield stress, the UHPC beams
302 reached its shear capacity. Then, following the theory of MCFT and taking into
303 account the contribution of the compression zone, the shear strength of the UHPC
304 beams with shear and moment can be obtained. Moreover, another 12 test results of
305 UHPC beams were selected for validation, specimen F series were tested by Zagon [24],
306 B25 and B50 specimens were tested by Amin [9]. Table 3 lists the shear strength of
307 UHPC beams predicted by the proposed method, traditional MCFT, and current
308 design codes of SETRA-AFGC [7] and SIA [8]. As can be seen, the stirrup ratio of the
309 UHPC beams has little effect on the shear strength, which mainly governed by the
310 shear span to depth ratio. The predictions of the proposed method have a good
311 agreement with the test results, the average Prediction/Test value is 0.92 and the
312 standard deviation is 7%. As for the UHPC beams with small shear span to depth ratio
313 ($\lambda < 2.5$), the design codes of SETRA-AFGC and SIA give an overly conservative
314 results, the mean Prediction / Test of the test specimen is just 0.69 and 0.71,
315 respectively. While for the case of $\lambda > 2.5$, SETRA-AFGC and SIA agree with the
316 test results, the mean value of the Prediction / Test is 0.83 and 0.85, respectively. That

317 is, the design codes of SETRA-AFGC and SIA only can be used to predict the shear
318 strength of the UHPC beams with $\lambda > 2.5$. Meanwhile, traditional MCFT method
319 will also underestimate the shear capacity of the UHPC beams with small span to
320 depth ratios, because the contribution of compression zones is neglected.

321 Fig.13 shows the shear capacity calculated by the proposed method of 156 tested
322 UHPC beams [10, 24-31]. The shear span ratio ranged from 1.0 to 3.5, and the stirrup
323 ratios varied from 0% to 3.42%. It can be seen that there is a certain discrepancy
324 between the predictions and test results, because the area of the vertical tie in truss
325 model is hard to define, which results a higher or a lower complementary energy. In
326 general, the average predicted shear capacity are close and generally reflect the test
327 results, the average value of $V_{pre} / V_{Test}$ is 0.88, and the standard deviation is 0.09.
328 Thus, the proposed method is a conservative method for designation.

329 Fig. 14 shows the effect of shear force and moment on shear strength of UHPC
330 beams with different shear span to depth ratios. As can be seen, when $\lambda < 0.75$, the
331 shear strength of UHPC beams is governed by the compressive strength of strut, while
332 $\lambda > 2.5$, the shear strength is controlled by the bending behavior of UHPC beams.
333 The shear strength decrease rapidly with the bending moment on the cross section.
334 However, this effect is not taken into account properly for current design codes, which
335 leads a conservative prediction.

## 336 Conclusions

337 A simply method is proposed to predict the shear capacity of UHPC beams with

small shear span to depth ratios based on the MCFT, the contribution of compression zone is taken into account based on the plastic theory. Moreover, the Mohr-Coulomb criterion for UHPC with shear and compression has been developed. The following conclusions can be drawn:

(1) The proposed method can predict the shear strength of UHPC beams with small shear span to depth ratios, the accuracy of the predictions has been validated by test. The mean values and standard deviation of the ratios of the experimental results to the predicted results based are 0.88 and 0.03, respectively.

(2) It can be seen that the current design codes of SETRA-AFGC and SIA give overly conservative values for shear strength of UHPC beams when the shear span to depth ratios is less than 2.5. Meanwhile, the predictions based on the traditional MCFT are conservative in most cases, because the contribution of compression zones is neglected.

(3) It should be noted that the UHPC beam failure occur due to concrete strut crushing when the shear to span ratio is less than 0.75, and the corresponding shear capacity can be predicted by the direct strut and tie model.

## Acknowledgments

This study was supported by the National Natural Science Foundation of China (Grant No. 51808208), the Fundamental Research Funds for The Central Universities (Grant No. 2242021R20011).

## Data Availability Statement

Some or all data, models, or code that support the findings of this study are available from the corresponding author upon reasonable request.

## References


[1] Graybeal, B.A. Compressive behavior of ultra-high-performance fiber-reinforced concrete. ACI Material Journal, 104(2): 146–152(2007).

[2] Ozyildirim, C. Evaluation of ultra-high-performance fiber-reinforced concrete. Virginia Center for Transportation Innovation and Research. Report No. FHWA/VCTIR 12-R1 (Federal Highway Administration, 2011).

[3] Wille, K., Naaman, A.E. & Montesinos, G.J. Ultra-high performance concrete with compressive strength exceeding 150MPa (22ksi): A simpler way. ACI Materials Journal, 108(1): 46–54(2011).

[4] Eric, S. Structural reliability of prestressed UHPC flexure models for bridge girders. Journal of Bridge Engineering, 15(1): 65–72(2010).

[5] Ashour, S.A., Wafa, F.F. & Kamal, M.I. Effect of the concrete compressive strength and tensile reinforcement ratio on flexural behavior of fibrous concrete. Engineering Structures, 22(9): 1145-1158(2000).

[6] Japan Society of Civil Engineers. Recommendation for design and construction of ultra-high strength concrete structures. (2006).

[7] AFGC. Ultra high performance fibre-reinforced concretes: AFGC/SETRA 2016. (France: AFGC/SETRA, 2016).

[8] SIA. Recommendation: Ultra-high performance fibre reinforced cement-based composites (UHPTRC): Construction material, dimensioning and application. (Lausanne, Switzerland, 2016).

[9] Amin, A. & Foster, S.J. Shear strength of steel fibre reinforced concrete beams with stirrups. Engineering Structures, 111(15): 323-332(2016).

[10] Thiemicke, J. & Fehling, E. Proposed model to predict the shear bearing capacity of UHPC-beams with combined reinforcement. 4th International symposium on ultra-high performance concrete and high performance construction materials, 62-63(2016).

[11] Preinstorfer, P. *et al*. Experimental investigation and analytical modelling of shear strength of thin walled textile-reinforced UHPC beams. Engineering Structures, 231(15): 111735(2021).

[12] Slater, E., Moni, M. & Alam, M.S. Predicting the shear strength of steel fiber reinforced concrete beams. Construction Building Material, 26(1): 423–436(2012).

[13] Ma, X.L., Chen, B.C. & Yang, Y. Calculation method of shear bearing capacity of R-UHPC beam. Journal of Traffic and Transportation Engineering, 17(5): 16-25(2017).

[14] Xu, H.B. & Deng, Z.C. Shear capacity of RPC beams based on modified pressure field theory. Journal of Hebei University of Technology, 43(6): 22-25(2014).

[15] Voo, Y., Poon, W.K. & Foster, S.J. Shear strength of steel fiber-reinforced ultra-high performance concrete beams without stirrups. Journal of Structural Engineering, 136(11): 1393-1400(2010).

[16] Vecchio, F.J. & Collins, M.P. The modified compression-field theory for reinforced concrete elements subjected to shear. ACI Structural Journal, 83(2): 219-231(1986).

[17] Charles, K.C. Shear and shear friction of ultra-high performance concrete bridge girders. (Georgia Institute of Technology, 2010).

[18] Stroeven, P. Stereological principles of spatial modeling applied to steel fiber-reinforced concrete in tension. ACI Materials Journal, 106(3): 216-222(2009).

[19] Kützing, L. Trafahigkeitsermittlung stahlfaserverstarkter betone, University of Leipzig, Germany, Stuttgart (2000).

[20] Abrishambaf, A., Pimentel, M. & Nunes, S. A meso-mechanical model to simulate the tensile behaviour of ultra-high performance fibre reinforced cementitious composites. Composite Structures, 222: 110911(2019).

[21] Yuan, H.Y. *et al*. Fracture energy of reactive powder concrete based on uniaxial tensile test. Advanced Materials Research, 306: 519-522(2011).

[22] Yang, J. & Fang, Z. Research on stress strain relationships of ultra-high performance concrete. Concrete, 7: 11-15(2008).

[23] Vecchio, F.J. & Collins, M.P. Predicting the response of reinforced concrete beams subjected to shear using the modified compression field theory. ACI Structural Journal, 3: 258-268(1988).

[24] Zagon, R., Matthys, S. & Kiss, Z. Shear behaviour of SFR-UHPC I-shaped beams. Construction and Building Materials, 124(15): 258-268(2016).

[25] Lim, D.H. & Oh, B.H. Experimental and theoretical investigation on the shear of steel fibre reinforced concrete beams. Engineering Structures, 21: 937-944(1999).

[26] Kwak, Y.K. *et al*. Shear strength of steel fiber-reinforced concrete beams without stirrups. ACI Structural Journal, 99(4): 530–538(2002).

[27] Calogero, C., Lidia, L. & Mendola, L. Effectiveness of stirrups and steel fibres as shear reinforcement. Cement and Concrete Composites, 26: 777-786(2004).

[28] Dinh, H., Montesinos, G. & Wight, J.K. Shear strength model for steel fiber reinforced

423 concrete beams without stirrup reinforcement. Journal Structure Engineering, 137(10): 1039–
424 1051(2010).
425[29] Ding, Y. *et al*. The composite effect of steel fibres and stirrups on the shear behaviour of
426 beams using self-consolidating concrete. Engineering Structures, 33: 107-117(2011).
427[30] Soetens, T. & Matthys, S. Shear design of full-scale prestressed SFRC girders. ACI-Fib
428 international workshop on fibre-reinforced concrete, Ghent University, Ghent, Belgium (2014).
429[31] Cai, G.H. *et al*. Shear capacity of steel fibre reinforced concrete coupling beams using
430 conventional reinforcements. Engineering Structures, 128: 428-440(2016).
431

# Figures

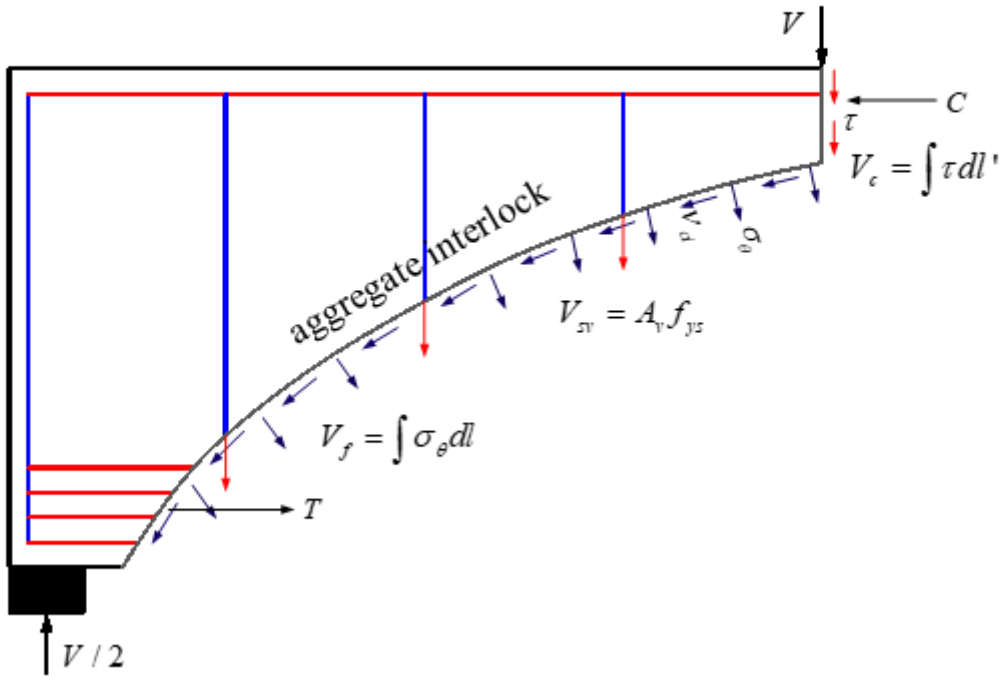


**Figure 1**

Shear forces on the cross section

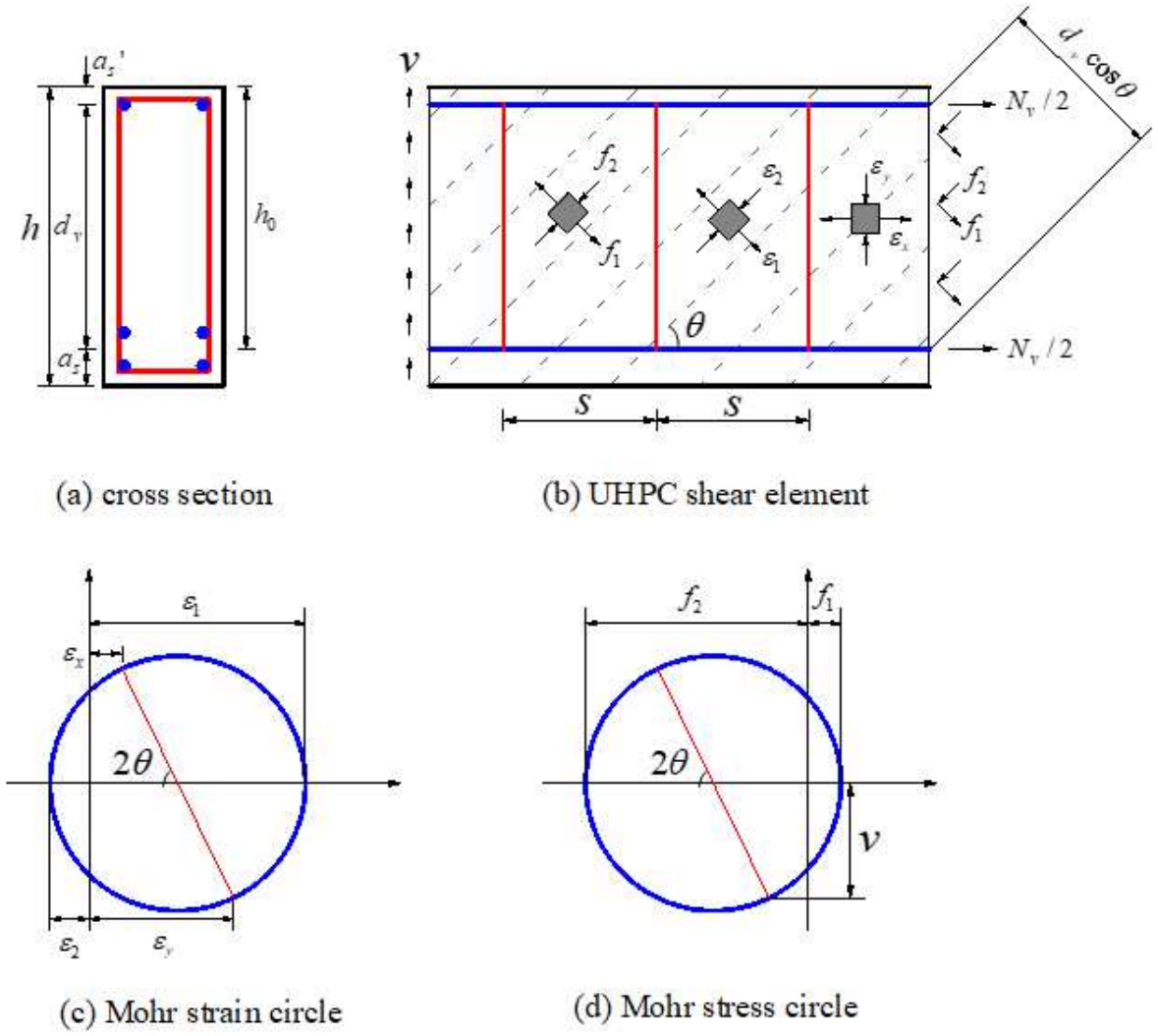


## Figure 2

Stress station of the UHPC elements under pure shear

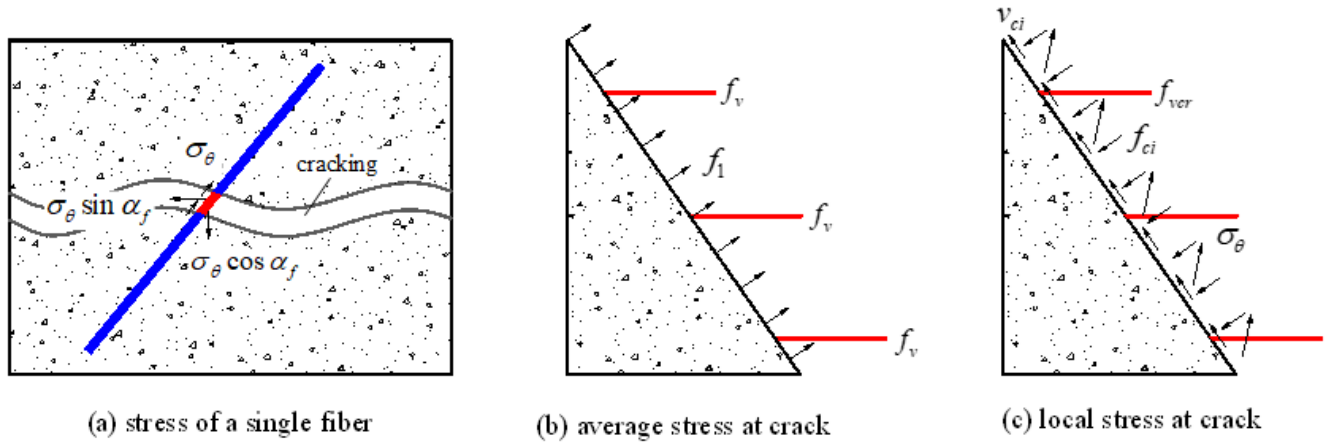


**Figure 3**

Stress condition at a crack

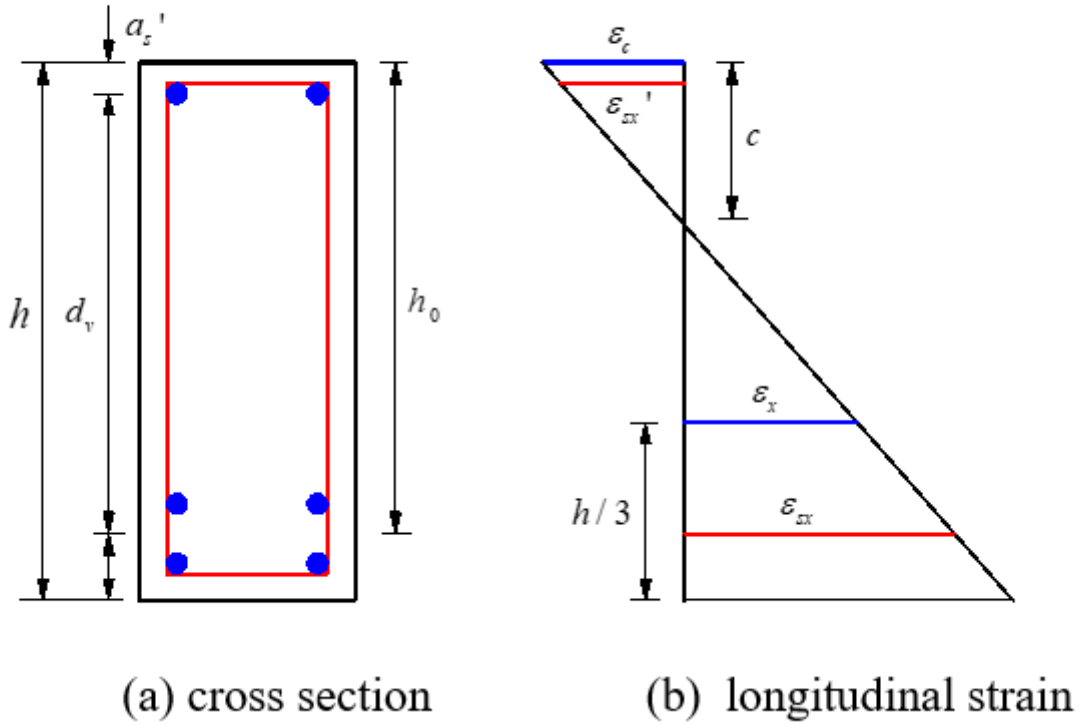


**Figure 4**

Distribution of the longitudinal strain at cross section; (a) cross section; and (b) longitudinal strain

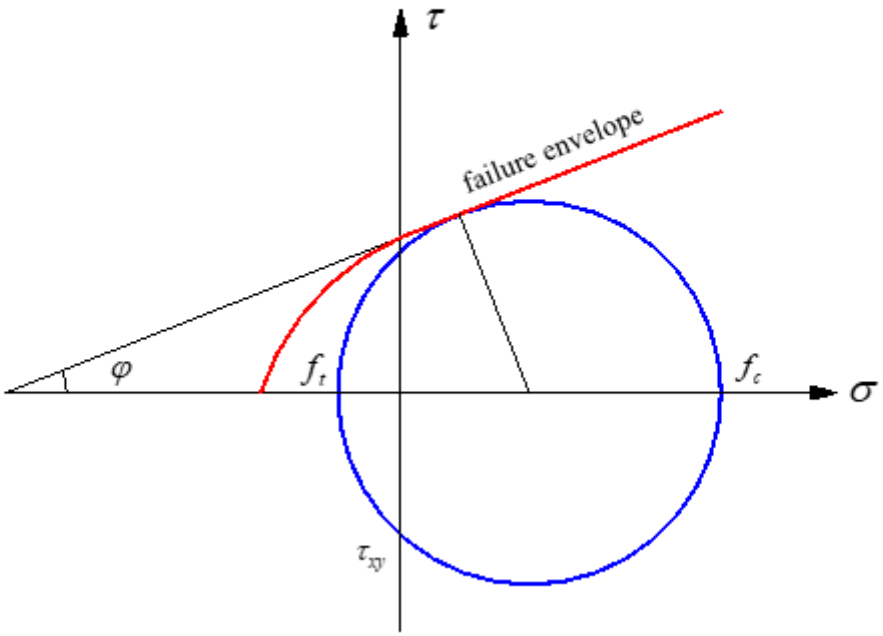


**Figure 5**

Mohr-Coulomb criterion for UHPC with shear and compression

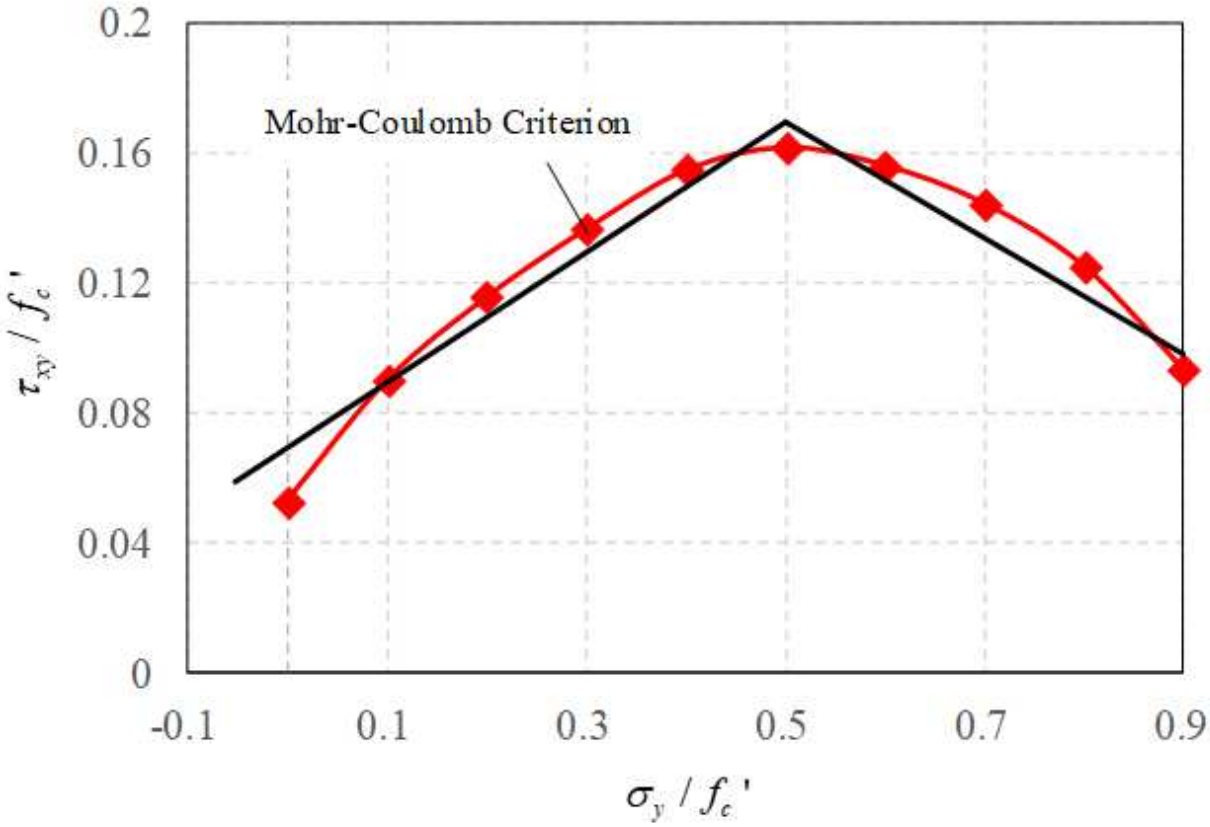


**Figure 6**

Mohr-Coulomb criterion of the UHPC under compression and shear

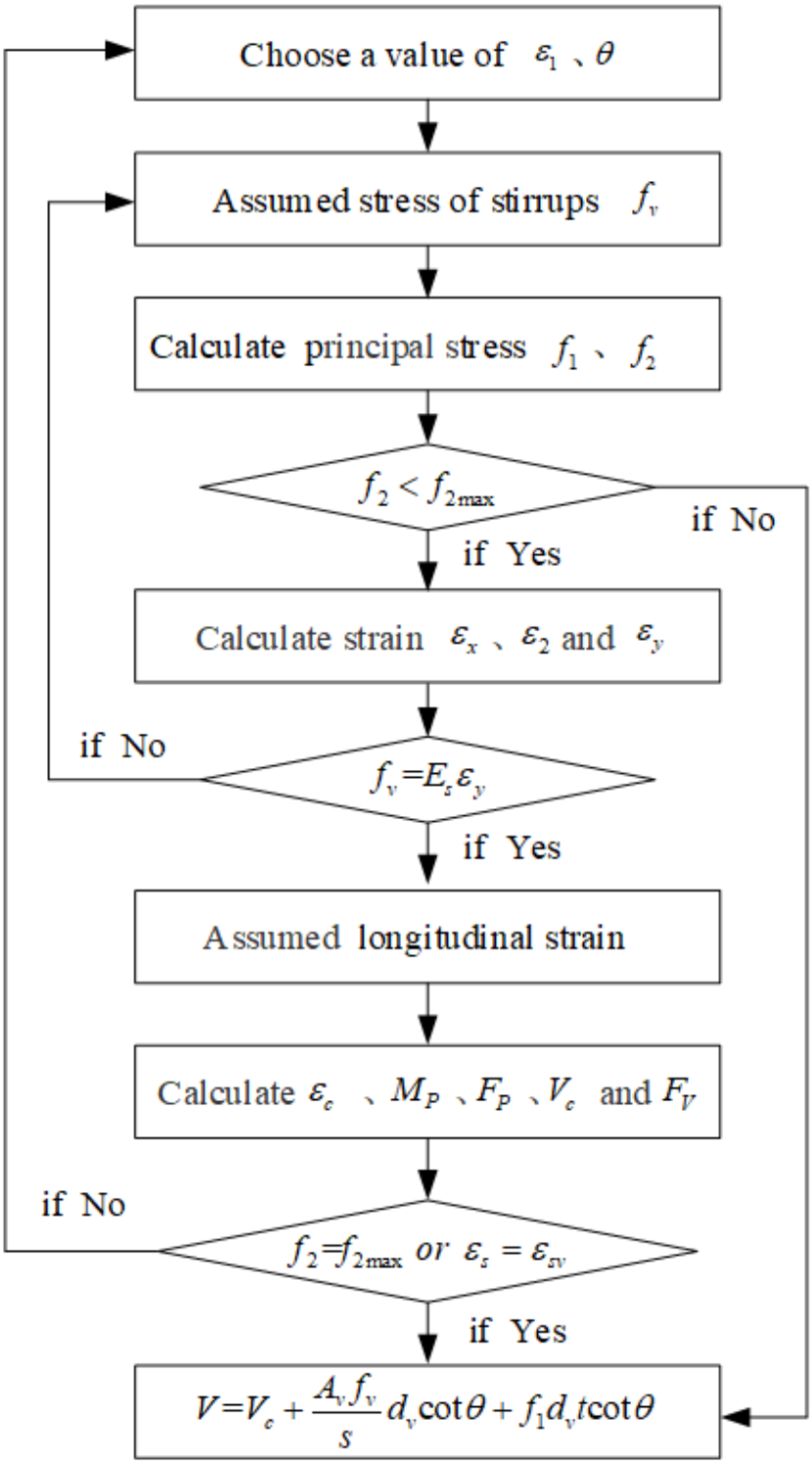


**Figure 7**

Modified MCFT model for UHPC members

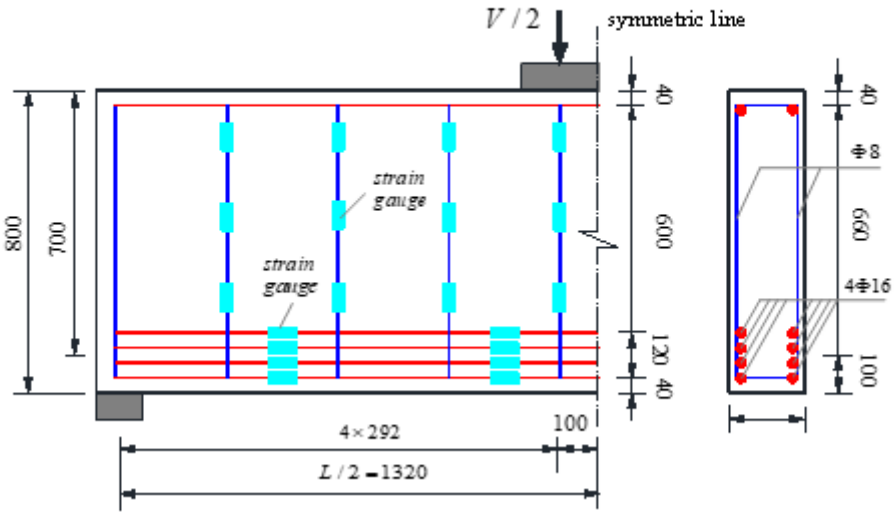


**Figure 8**

Stress-strain relationships of the UHPC with reinforcement

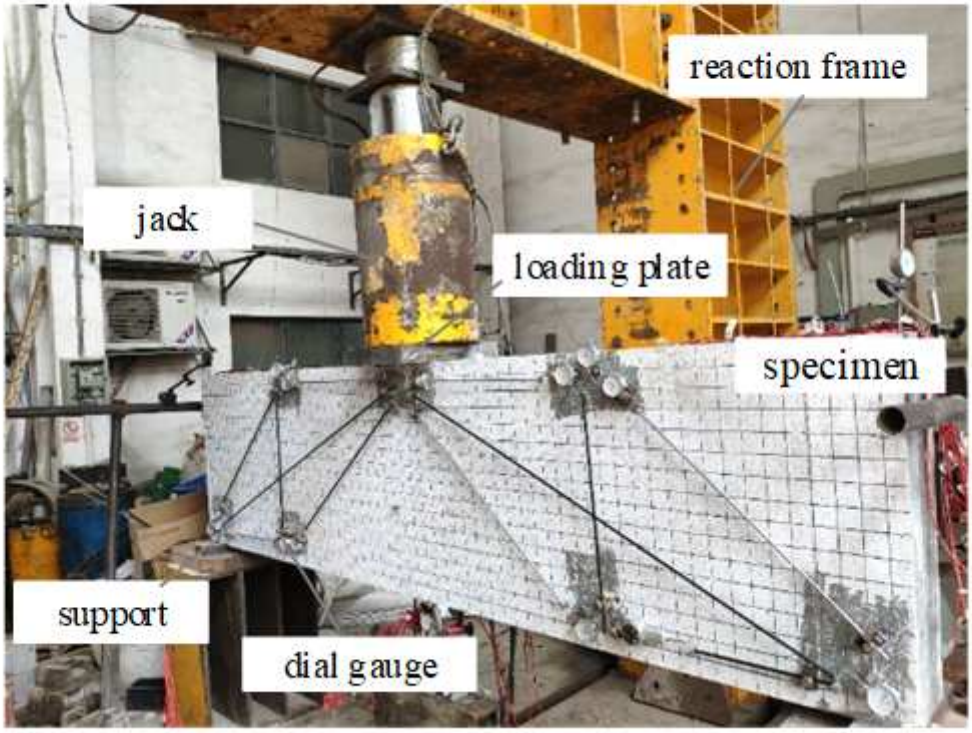


**Figure 9**

Test of the UHPC specimens

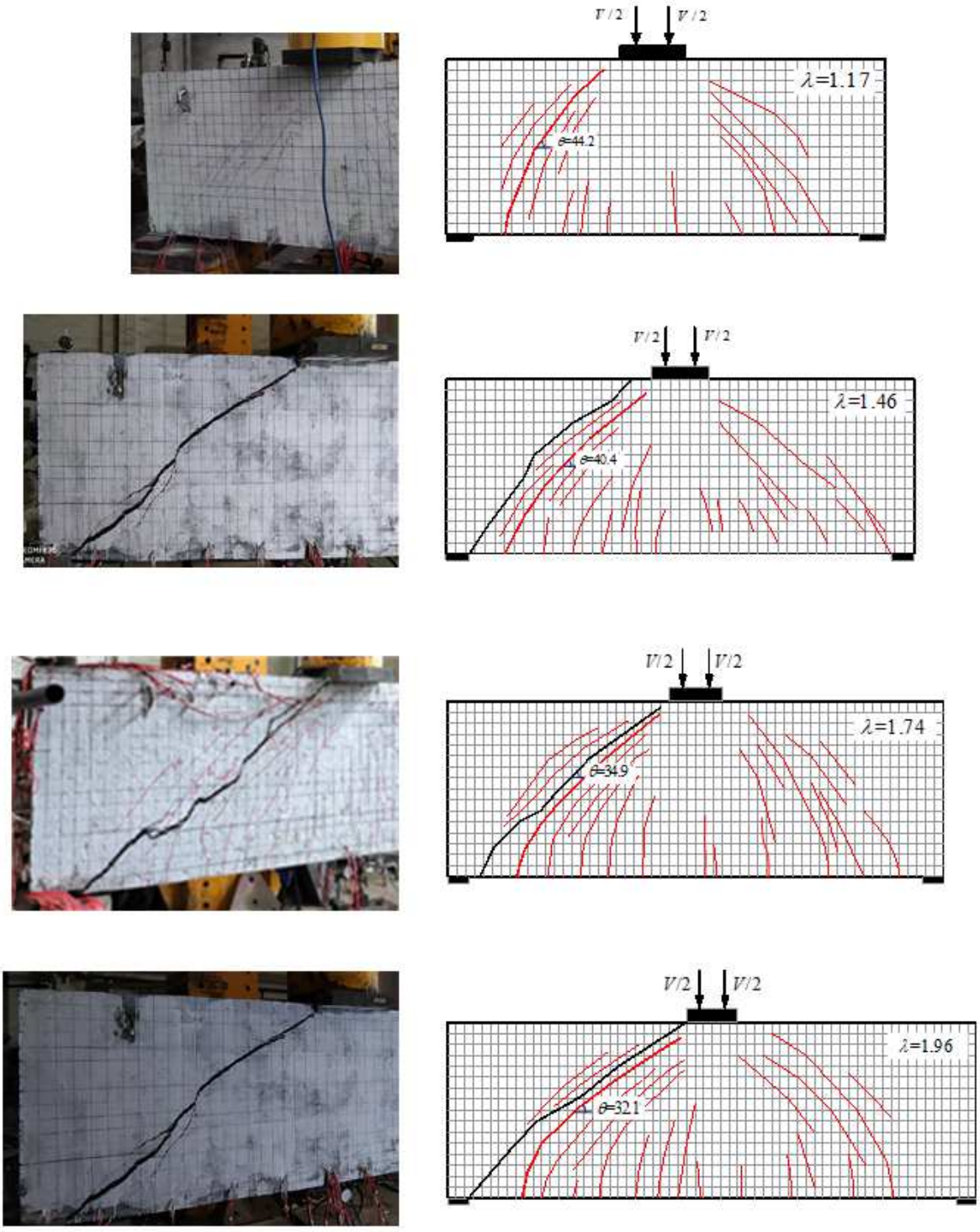


**Figure 10**

Crack pattern of the specimen

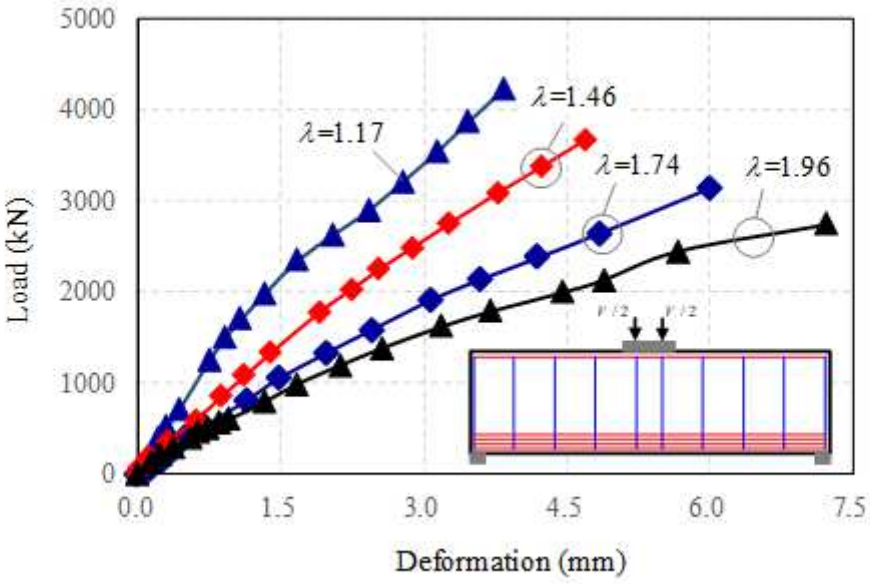


**Figure 11**

Load vs deformation of the test specimen

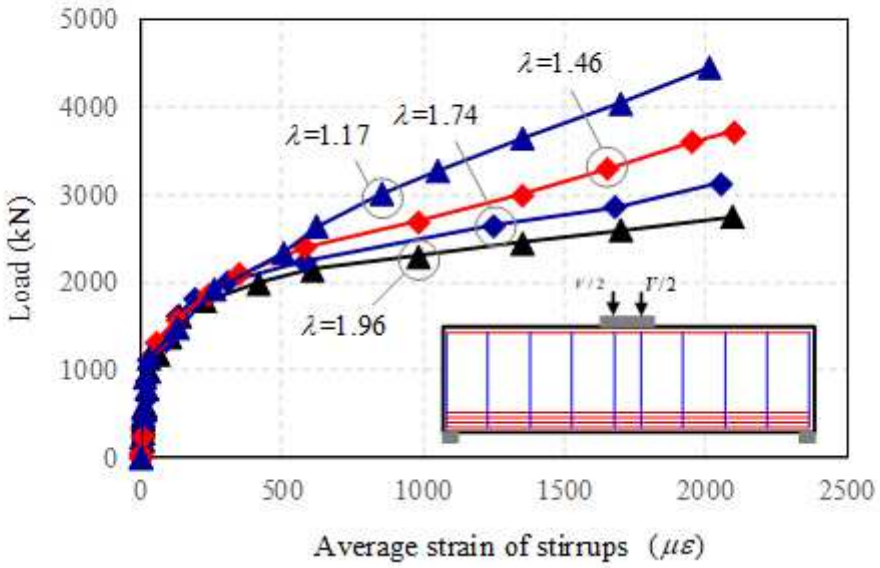


**Figure 12**

Average strain of the stirrups

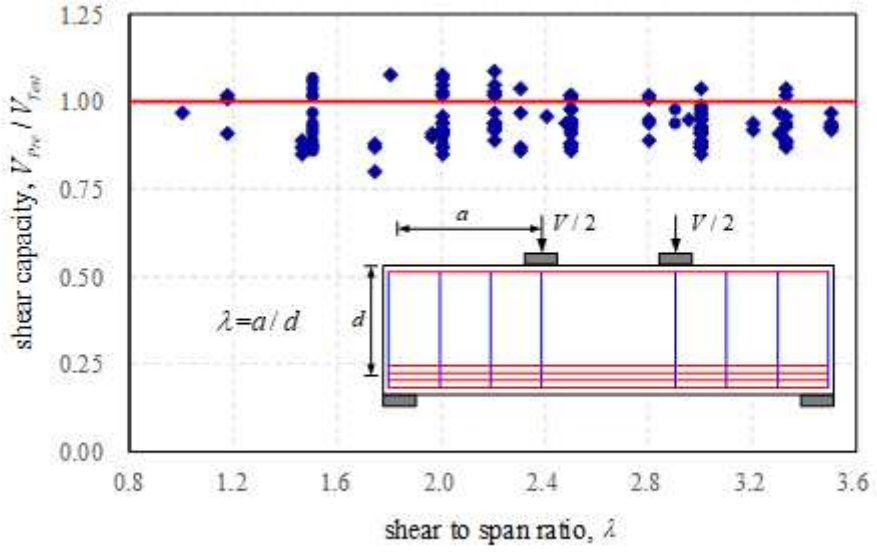


**Figure 13**

Shear capacity of the UHPC beams with different shear to span ratios

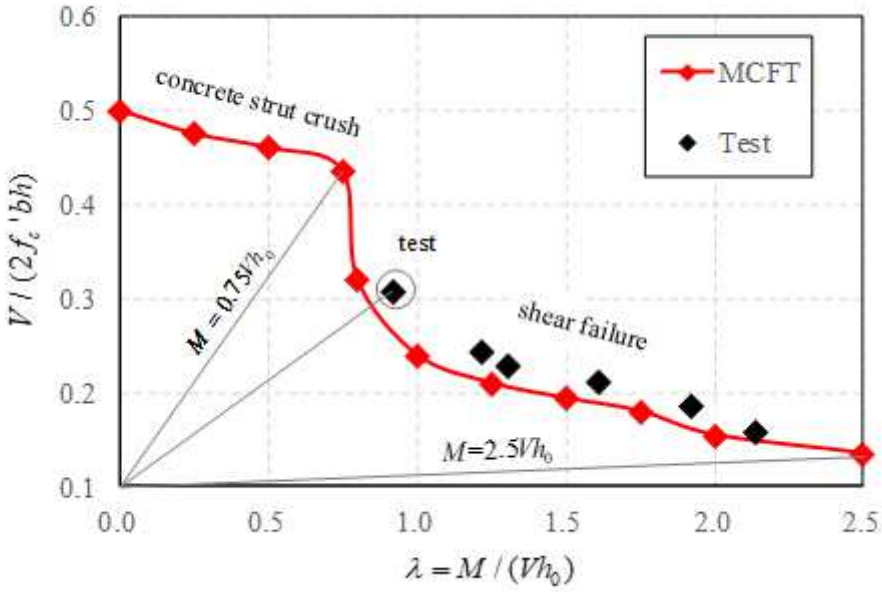


**Figure 14**

Shear strength of UHPC beams with shear force and bending moment